Skyrmion Fluid and Bimeron Glass Protected by a Chiral Spin Liquid on a Kagome Lattice

H. Diego Rosales, Flavia Albarracín, Pierre Pujol, Ludovic D. C. Jaubert

A skyrmion fluid and bimeron glass emerging from competition with a chiral spin liquid

H. Diego Rosales,[1,2,3] Flavia A. Gómez Albarracín,[1,2,3] Pierre Pujol,[4] and Ludovic D. C. Jaubert[5]

[1] *Instituto de Física de Líquidos y Sistemas Biológicos, CONICET, Facultad de Ciencias Exactas, Universidad Nacional de La Plata, 1900 La Plata, Argentina*
[2] *Departamento de Física, FCE, UNLP, La Plata, Argentina*
[3] *Departamento de Ciencias Básicas, Facultad de Ingeniería, UNLP, La Plata, Argentina*
[4] *Laboratoire de Physique Théorique, CNRS and Université de Toulouse, UPS, Toulouse, F-31062, France*
[5] *CNRS, Université de Bordeaux, LOMA, UMR 5798, 33400 Talence, France*

(Dated: February 14, 2022)

Skyrmions are of interest both from a fundamental and technological point of view, due to their potential to act as information carriers. One great challenge concerns their manipulation and control, especially at higher temperatures. Here we combine skyrmion physics with another aspects of modern condensed matter: spin liquids. Using the high entropy and broken symmetry of a chiral spin liquid, we design a theoretical model to control the density of well defined skyrmions with temperature, all the way from a diluted gas to a dense liquid and a crystallised solid. At high field, the skyrmion fluid forms an original bimeron glass with high degeneracy and out-of-equilibrium dynamics, reminiscent of co-polymer physics and chain models in statistical mechanics. Our approach illustrates how spin-liquid properties can be used for the design of tailored models, and further connects skyrmions to phenomena beyond condensed matter.

Experimental evidence for the existence of skyrmions is well established [1–5]. Their topological charge provides them with enhanced stability and potential applications in the next-generation information storage and processing devices [6, 7]. In that context a dilute phase of skyrmion has been proposed as framework for a true random seed generator [8, 9]; a prospect that has recently spurred the search for mechanisms to stabilise such a dilute phase [10, 11].

The conventional route to skyrmions involves competing interactions between, for example, symmetric Heisenberg and antisymmetric Dzyaloshinskii-Moriya interactions. Skyrmions typically appear as an intermediate phase when increasing the magnetic field, between a helical (H) phase and a field-polarised (FP) regime [12, 13], where they condense to form a two-dimensional periodic array (SkX) embedded in a ferromagnetic [14–16] or antiferromagnetic [17–21] background. The magnetic field is thus a useful parameter to control the density of skyrmions, a property recently used to study the historical question of two-dimensional melting in a modern setting [22–24]. In contrast, heating does not only melt the SkX phase [22, 25, 26] but also usually decomposes each individual skyrmion as an entity, as they adiabatically connect to a structureless paramagnet (see illustration in video S1). Theoretical models where the density of well-defined skyrmion quasi-particles can be controlled at high temperature are not trivial.

Our motivation here is to modify the generic phase diagram of skyrmion crystals [27] [Fig. 1.(a)] and to design a microscopic, original, model where skyrmion density can be gradually controlled by temperature, all the way from the melting of the SkX phase to a vanishing density. A necessary but not sufficient condition for this to happen is that skyrmions have to remain well defined entities above the SkX melting. Designing such model would be a useful step in learning how to manipulate these topological textures, and exploring the physics of a skyrmion fluid through multiple parameters, all the way from a dilute gas to a dense liquid, and, as we shall see, an unconventional form of glass.

Presentation. The idea is to partially *encircle* the SkX phase with the FP regime as illustrated in Fig. 1.(a,b). Since the magnetic field breaks time-reversal symmetry, the FP regime is connected to the paramagnetic phase via a crossover, and not a thermodynamic phase transition. Nonetheless, thermal fluctuations responsible for skyrmions are strongly suppressed in the FP regime. Hence, the circumventing FP regime can be interpreted as a quasi vacuum of skyrmions, here imposed at temperatures above the SkX phase. Cooling down at fixed field from the FP region, skyrmions are spontaneously created, first forming a dilute gas, then a dense liquid before crystallising into the SkX solid.

While appealing, this idea leaves us with one important open question: how to stabilise the field-polarised regime at lower field and high temperature as depicted in Fig. 1.(b) ? To do so, we shall combine skyrmion physics with another fundamental concept in condensed matter: spin liquids [28]. In their classical form, spin liquids possess a large entropy at little if no energy costs, that might just rival with the free energy of a paramagnet in a field. Beyond skyrmion physics, our work thus offers a alternate take on spin liquids. Here we are not investigating their existence or describing their properties, as is common in literature; we are rather using them as a tool to design the phase diagram we are looking for.

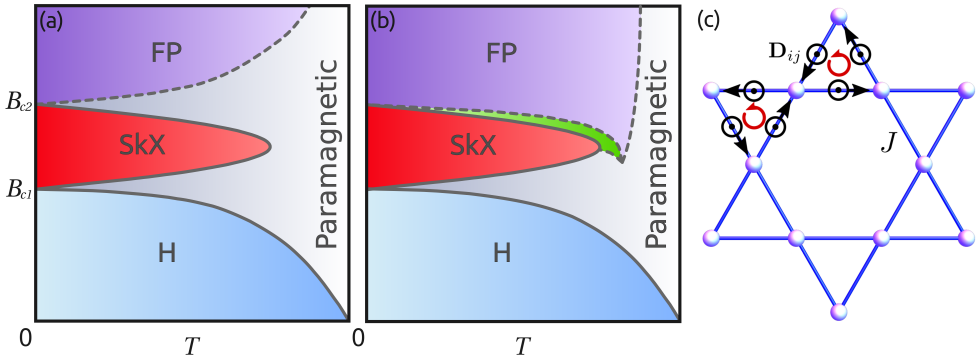

FIG. 1. **How to tune the skyrmion density.** **(a)** Schematic representation of the traditional phase diagram where the magnetic field destroys the skyrmion crystal (SkX) in favour of a field-polarised (FP) regime with no skyrmions. **(b)** Illustration of our idea where the FP phase is brought down at high temperature, circling around the SkX phase, imposing a region with no skyrmions and thus creating an intermediate regime (in green) where their density can be tuned gradually. Solid and dashed lines respectively indicate transitions and crossovers. **(c)** To bring down the FP regime at high temperature, we shall use the large entropy of a ferromagnetic spin liquid on the kagome lattice with nearest-neighbour Heisenberg exchange and Dzyaloshinskii-Moriya interactions.

We shall now explain how to practically merge these different elements into a microscopic Hamiltonian.

Construction of the model. The first question we are facing is that models for spin liquids are usually antiferromagnetic in nature, which is a priori incompatible with the field-polarised (FP) regime. Actually, the very co-existence of ferromagnetic order and spin liquid seems paradoxal. Fortunately there are a few counter-examples among the so-called chiral spin liquids [29, 30] where a disordered fraction of magnetic degrees of freedom co-exists with broken time-reversal symmetry. Here we will consider a known classical chiral spin liquid on the kagome lattice [31] [Fig. 1.(c)]

$$\mathcal{H}_{\rm SL} = -\sum_{\langle i,j\rangle} \mathbf{S}_i \cdot \mathbf{S}_j - \sqrt{3}\,\mathbf{z}\cdot(\mathbf{S}_i \times \mathbf{S}_j). \qquad (1)$$

where $\mathbf{S}_i$ are classical Heisenberg spins of unit length ($|\mathbf{S}_i| = 1$), $\langle i,j\rangle$ is a sum over all nearest neighbours and $\mathbf{z}$ is the out-of-plane unit vector. The second term corresponds to out-of-plane Dzyaloshinskii-Moriya interactions with strength $D^z = \sqrt{3}$. The ground state of this Hamiltonian is a chiral spin liquid that combines the extensive degeneracy of the three-colouring problem on kagome for the in-plane spin components [32] with out-of-plane ferromagnetism [31, 33].

In order to stabilise skyrmions, the Heisenberg ferromagnetic coupling of Hamiltonian [1] is a good start, but *in-plane* Dzyaloshinskii-Moriya interactions $D^\perp$ are also typically required [see Fig. 1.(c)]. $D^\perp$ competes with ferromagnetism [Fig. 2.(a)] and the chiral spin liquid makes way for a labyrinth [Fig. 2.(c)] and helical (H) phases [4, 12]. For example at $D^\perp = 0.5$, we find that the chiral spin liquid has disappeared for all temperatures.

The last step is to turn on the magnetic field B along the $\mathbf{z}$ direction, for two reasons. First, this is the standard procedure to produce a SkX phase at intermediate field values [12]. And at the same time the Zeeman term favours ferromagnetism, and thus, hopefully, the chiral spin liquid.

In summary, our Hamiltonian is

$$\mathcal{H} = -\sum_{\langle ij\rangle} [J\,\mathbf{S}_i \cdot \mathbf{S}_j - \mathbf{D}_{ij}\cdot(\mathbf{S}_i \times \mathbf{S}_j)] - B\sum_i S_i^z, \qquad (2)$$

where $\mathbf{D}_{ij} = D^z\,\mathbf{z} + D^\perp\,\mathbf{e}_{ij}$ with $\mathbf{e}_{ij} = (\mathbf{r}_j - \mathbf{r}_i)/|\mathbf{r}_j - \mathbf{r}_i|$ the unit vector between two neighbouring sites $\langle ij\rangle$ [Fig. 1.(c)]. At no loss of generality, we shall set the energy scale of the system with $J = 1$. To keep the chiral spin liquid $\mathcal{H}_{\rm SL}$ at proximity in parameter space, we fix $D^z = \sqrt{3}$. And finally, unless specified otherwise, we fix $D^\perp = 0.5$ in order to stabilise a helical phase at zero field [Fig. 2.(a)]. To properly account for the nature of the chiral spin liquid, we use classical Monte Carlo simulations.

Competition between two chiral phases. Upon increasing the field, the helical phase becomes the skyrmion solid at $B \approx 0.04$, with a thin intervening region in between [Fig. 2.(b)] where bimerons are known to co-exist with skyrmions [27], as illustrated in Fig. 2.(d). A skyrmion can be described as the juxtaposition of two merons, each of them carrying half the topological charge. Two merons are able to separate, leaving a trail of spins opposite to B connecting these two halves of the topological charge [Fig. 5.(c)]. Another way to understand bimerons is as an intermediate step, as the one-dimensional stripes of the helical phase decompose into an array of skyrmions, stabilised by thermal fluctuations [27, 34].

But what happens at intermediate field ? One of the main outcomes of our work is that the idea schematically

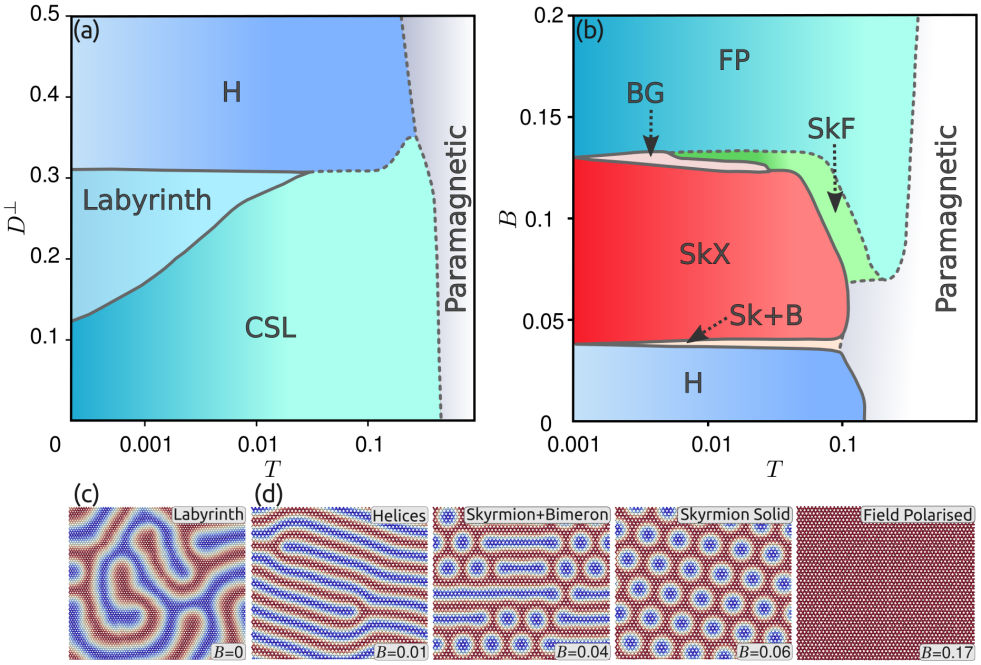

FIG. 2. **Phase diagrams** of Hamiltonian [2] for (a) $B = 0$ and (b) $D^\perp = 0.5$. **(a)** In zero field, the chiral spin liquid (CSL) of Hamiltonian [1] is suppressed for large values of $D^\perp$, in favour of a helical (H) phase. **(b)** Starting from this helical phase for $D^\perp = 0.5$, an external magnetic field B forms a skyrmion lattice (SkX) and then a field-polarised (FP) phase. The later is actually a resurgence of the (ferromagnetic) chiral spin liquid. The important result is that the chiral spin liquid circles around the SkX phase at high temperature, creating an intermediate skyrmion-fluid region (SkF, in green) where the density of skyrmion can be tuned with temperature from a diluted gas to a dense liquid. Just below and above the SkX phase in field, we have two different bimeron regimes. The former is standard [27] while the latter is a "bimeron glass", with extended bimerons that occupy a large portion of the system [Fig. 5]. Solid and dashed lines respectively indicate thermodynamic transitions and crossovers, with the caveat that the metastability of the bimeron glass makes it difficult to ascertain the nature of the boundaries; a first-order transition is possible, especially at low temperature. **(c)** Snapshots of a labyrinth spin configuration in panel (a) at $B = 0$ and $D^\perp = 0.2$. **(d)** Snapshots of spin configurations representative of different regions of the phase diagram in panel (b): the helical phase at $B = 0.01$, the bimeron + skyrmion regime at $B = 0.04$, the skyrmion solid at $B = 0.06$ and the FP regime at $B = 0.17$.

presented in Fig. 1.(b) essentially works for Hamiltonian [2]. At low temperature and high field, the chiral spin liquid reappears in the FP regime. The way our model deviates from the traditional picture of Fig. 1.(a) is that the FP regime persists upon heating at *lower* fields, encircling part of the SkX phase. This is quantitatively explained in Fig. 3 for $B = 0.09$.

The specific heat C_h presents two peaks. Upon cooling, the first one indicates the crossover from standard paramagnetism to the spin-liquid regime; after this peak, C_h becomes smaller than 1, an indication of soft modes frequently observed in spin liquids with classical Heisenberg spins [35]. This first peak is accompanied by a clear increase of the magnetisation M_z, as expected for a field-polarised regime. Then M_z presents a sharp upturn at the same temperature T_g than C_h reaches its minimum. T_g marks the end of the spin-liquid regime and the apparition of a skyrmion gas, whose number of skyrmions N_{sk} increases smoothly until reaching saturation at T_l. In this temperature window, $T_l < T < T_g$, we are thus able to achieve our goal and tune the density of skyrmions from zero to saturation.

While the number of skyrmions remains essentially constant below T_l, it does not mean that they immediately form an ordered array. To measure the onset of order, we define the orientational order parameter [22–24, 26]

$$\Psi_6 = \left| \frac{1}{N_{sk}} \sum_{i=1}^{N_{sk}} \frac{1}{n_i} \sum_{j=1}^{n_i} e^{i\,6\theta_{ij}} \right| \qquad (3)$$

where θ_{ij} is defined in the inset of Fig. 3.(b) and n_i is the number of nearest neighbours (labelled j) surrounding skyrmion i as determined by Delaunay triangulation. For the triangular geometry of the SkX solid, $n_i = 6$ and $\theta_{ij} = \pi/3$ implies that $\Psi_6 = 1$. In Fig. 3.(b), Ψ_6 shows that the SkX solid phase only appears at T_s, clearly below the second peak of specific heat, offering a range of temperature, $T_s < T < T_l$, for a dense liquid of skyrmions. Video S2 shows this evolution from a skyrmion gas to a skyrmion solid upon cooling, as opposed to video S1 where skyrmions appear out of

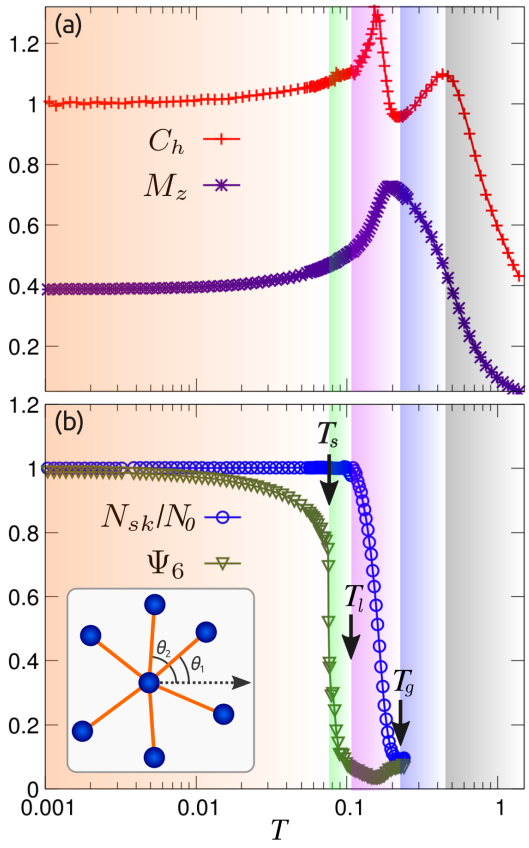

FIG. 3. **Competition between the chiral spin liquid and skyrmion solid** at $B = 0.09$ as measured from: **(a)** the specific heat C_h and magnetisation M_z, **(b)** the normalised number of skyrmion N_{sk} and orientational order parameter Ψ_6 defined in Eq. [3]. The chiral spin liquid disappears at T_g when the number of skyrmions start to grow. The density of skyrmion can be tuned by the temperature between T_g and T_l. **Inset:** Definition of the angle θ_{ij} used in the orientational order parameter of Eq. [3].

paramagnetic fluctuations. Since the only difference in Hamiltonian parameters between videos S1 and S2 is that $D^z = 0$ and $D^z = \sqrt{3}$ respectively, the importance of the chiral spin liquid of Hamiltonian [1] is clearly established.

To further confirm that the FP regime is dominated by the spin liquid, we compute the structure factor from simulations at $B = 0.09$ (see Appendix). As a general principle, a spin liquid corresponds to the manifold of spin configurations respecting a given set of local constraints that minimises the energy. In reciprocal space, this manifold takes the form of flat bands while the constraints impose characteristic features in the structure factor. For the chiral spin liquid of Hamiltonian [1], these features are pinch points [31]. At $T = 0^+$ pinch points are singularities at the centre of Brillouin zones, but at high temperature they are broadened by thermal fluctuations. The observation of these broad pinch points in Fig. 4.(e) confirms the underlying spin-liquid origin of the FP region at high temperature.

Remarkably, a somewhat unexpected outcome is the apparition of half-moon patterns in the skyrmion-gas regime [Fig. 4.(f)]. These patterns have been observed in a variety of systems: inelastic neutron scattering experiments of $Tb_2Ti_2O_7$ [36] and $NaCaNi_2F_7$ [37], as well as simulations of kagome [38] and spin-ice models [39, 40], and models parametrised for $Nd_2Zr_2O_7$ [41] and the kagome bi-layer spin liquid $Ca_{10}Cr_7O_{28}$ [42, 43]. In a nutshell, when a spin liquid supports flat bands with pinch points, half moons may appear in the inelastic structure factor at finite energy [38, 41]. However, when observed in the equal-time structure factor [44], as it is the case in Fig. 4.(f), half moons indicate that the spin-liquid flat band(s) lie at higher energies above the ground state. Thermal fluctuations are not enough to populate them. The structure factor becomes dominated by dispersive bands of lower energy that carry the half moons. In other words, the flat bands play the role of an entropic buffer that stabilise the field-polarised region at high temperature [Fig. 4.(a,e)]. But as you cool down the system, flat bands become depopulated and the FP region disappears. This gives rise to the apparition of skyrmions in real space [Fig. 4.(b)] and half moons in reciprocal space [Fig. 4.(f)]. Upon further cooling, the half moons "close" into the shape of a circle [Fig. 4.(g)] as expected for a fluid of quasi-particles [Fig. 4.(c)] [23, 25, 26]. Finally, the traditional Bragg peaks with six-fold symmetry appear in the SkX phase [Fig. 4.(d,h)].

Bimeron glass. For $B \approx 0.13$, there is a noticeable regime where the skyrmion fluid persists down to very low temperature [Fig. 2.(b)]. The field is not high enough to suppress all skyrmions, but their number is too low to form a solid. As opposed to traditional models in this regime [22–24], skyrmions become unstable upon cooling. They split into two merons, forming extended bimerons spanning the entire system [see Fig. 5 and video S3]. These one-dimensional textures are sometimes referred to as "snakes" in the literature [45–47]. Once nucleated, the growth of bimerons in this field regime is almost instantaneous in our simulations, occupying the empty space between pre-existing skyrmions. The resulting spin configurations is then frozen in a pattern related to the proximate SkX solid. Colloquially speaking, it is as if the bimerons were "connecting the dots" of the triangular SkX array. Different initial seeds in simulations always give different, frozen, states at low temperatures (see Fig. 5.(a,b) and the out-of-equilibrium dynamics in video S3). We coin this regime a *bimeron glass* (BG).

The frozen arrangement of bimerons and skyrmions is similar to Hamiltonian chains [48], where each vertex of the lattice is visited exactly once by a bimeron or skyrmion [49]. As a Hamiltonian-chain analogue, it possesses an extensive and countable degeneracy, with potential to store information. In that context,

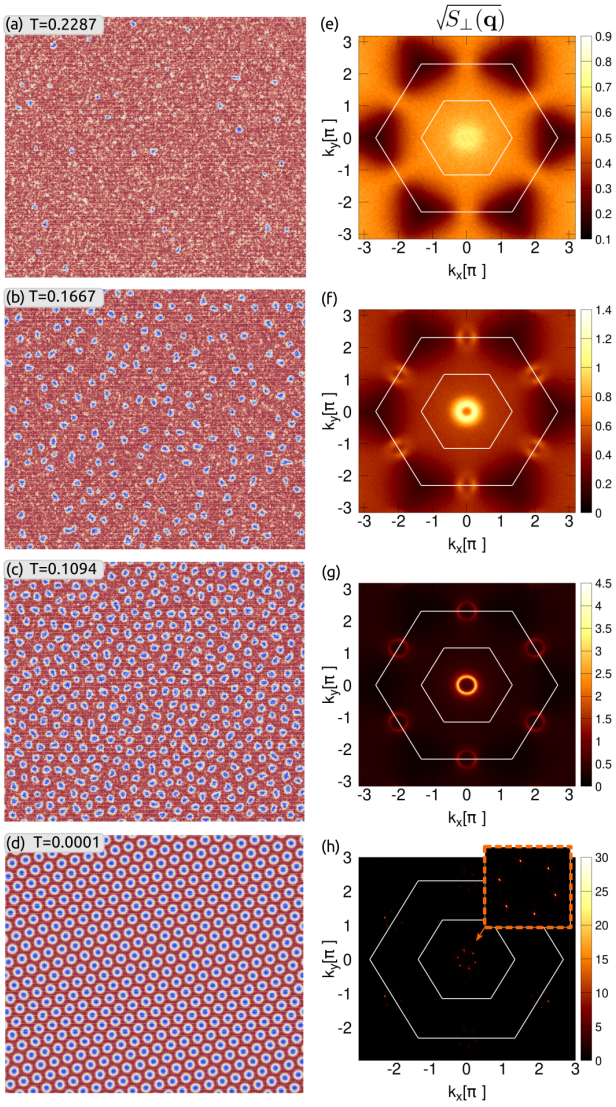

FIG. 4. **From SkX to chiral spin liquid in real and reciprocal space at $B = 0.09$. (a-d)** Snapshot of spin configurations at different temperatures T. **(e-h)** Equal-time structure factor $\sqrt{S_\perp(\mathbf{q})}$ at the same temperatures showing the characteristic Bragg peaks/circle/half moons and broad pinch points of the skyrmion solid/liquid/gas and field-polarised chiral spin liquid respectively.

the frozen dynamics offers a welcome stability to the bimeron/skyrmion configuration at fixed field. Stepping away from magnetic materials, hamiltonian chains also share interesting statistical properties with polymer melting [50] and protein folding [51]. In particular, the patterns of Fig. 5 are reminiscent of the intermediate dynamical regime in the order-order transition of copolymer thin films [52]. These connections between skyrmions and other branches of physics are promising, and further work is needed to investigate this peculiar type of glass, made of zero- and one-dimensional topological defects.

Conclusion We have designed a microscopic model, starting from a known ferromagnetic chiral spin liquid in the kagome lattice. To stabilize skyrmions, we included two key ingredients: in-plane Dzyaloshinskii-Moriya and a magnetic field. This simple model deviates from the traditional phase diagram of skyrmions. In particular, at intermediate magnetic fields, temperature serves as a control parameter for the number of skyrmions. Upon cooling, a sequence of magnetic textures is stabilised, starting from a dilute gas, going through a liquid until reaching a solid phase of skyrmions. This diversity of textures also stands out in reciprocal space where the presence of pinch-points and half-moons confirms the influence of the chiral spin liquid. Before setting into a fully magnetised regime, a "bimeron glass" emerges at low temperature where bimerons and skyrmions co-exist forming a singular lattice with frozen dynamics in simulations.

Our work opens the path for a variety of research directions, from the manipulation of the skyrmion fluid to the glassy dynamics of the bimeron glass, with connection to diverse branches of physics. It also brings to light another example of half-moon patterns in reciprocal space, of recent interest in spin-liquid research, with the notable advantage of being attached to a clear phenomenon, namely the emergence of skyrmions. More generally, the competition between multiple chiral phases is expected to show peculiar signatures in transport properties, e.g. in thermal and anomalous Hall effects.

To conclude, we should mention that the spin liquid of Hamiltonian [1] can be mapped exactly onto a specific point XXZ_0 of the XXZ Hamiltonian on the kagome lattice with in-plane antiferromagnetic coupling, connected to a network of spins liquids [31]. This mapping only transforms in-plane spin components which means that while the $D^\perp$ term would be rotated, the magnetic field along the $z-$axis is invariant. Hence, all the physics presented in this paper can be exactly transposed onto the XXZ_0 kagome model with rotated in-plane Dzyaloshinskii-Moriya interactions and $D^z = 0$. And the consequences of the remarkable quantum properties of the XXZ_0 model [53, 54] on the skyrmion fluid is a vast and open question.

Acknowledgments. We thank Leticia Cugliandolo, Santiago Grigera and Peter Holdsworth for useful comments. H.D.R. and F.A.G.A. acknowledge financial support from CONICET (PIP 2021-11220200101480CO) and SECyT-UNLP (I+D X893) and F.A.G.A. from PICT 2018-02968. L.D.C.J. acknowledges financial support from the "Agence Nationale de la Recherche" under Grant No.ANR-18-CE30-0011-01.

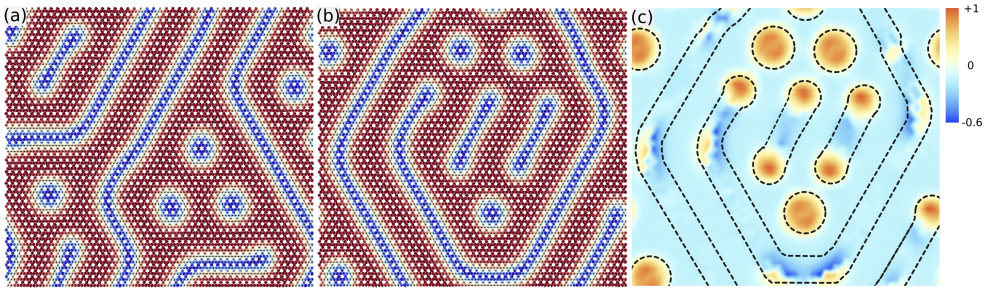

FIG. 5. **Snapshots of the bimeron glass** at $T = 10^{-3}$ and $B = 0.13$ (panels (a) and (b)). These snapshots are obtained at the end of Monte-Carlo simulations where the system is essentially frozen, from two different initial spin configurations. Topological charge density corresponding to spin configuration (b) is encoded by colours (blue for negative and red for positive) in panel (c), showing that the topological charge is concentrated at the ends of the bimerons (the merons).

Appendix

Monte Carlo simulations. Monte Carlo simulations were performed using the Metropolis and Heat-bath algorithms combined with overrelaxation (microcanonical) updates. We use an annealing scheme to lower the temperature (T) at fixed external magnetic field (B) and computing 200 independent runs initialized by different random numbers for each T and B. Simulations were performed in $N_c = 3 \times L^2$ magnetic site clusters, with $L = 48 - 192$ and periodic boundary conditions. $10^5 - 10^6$ Monte Carlo steps (MCS) were used for initial relaxation, and measurements were taken in twice as much MCS.

Topological charge. We use the colour bar, as indicated in Fig. 5(c) of the main text, to encode the local topological charge or skyrmion charge density defined as $\chi_n = \mathbf{S}_i \cdot (\mathbf{S}_j \times \mathbf{S}_k)$ where n indexes a elementary triangle of sites i, j and k in the kagome layer.

Skyrmion positions. Assuming a skyrmion phase as an assembly of quasiparticles, we first identify individual skyrmions considering the spins clusters where $S_i^z < 0$. Then, we can define the position of skyrmion j in a magnetic texture as

$$\mathbf{R}_j = \frac{1}{N_{cluster}} \sum_{i \in \text{cluster}} \mathbf{r}_i, \tag{4}$$

where $N_{cluster}$ is the number of sites in a spin cluster defining the skyrmion, and $\mathbf{r}_i$ denotes the lattice point vector of site i.

Structure factor. The structure factor $S_\perp(\mathbf{q})$ is

$$S_\perp(\mathbf{q}) = \frac{1}{N_c} \sum_{a=x,y} \langle | \sum_j S_j^a e^{i\mathbf{q}\cdot\mathbf{r_j}} |^2 \rangle, \tag{5}$$

where the summation is over all kagome sites j and for the in-plane spin components only to avoid the Bragg peaks coming from the magnetic field.

[1] S. Mühlbauer, B. Binz, F. Jonietz, C. Pfleiderer, A. Rosch, A. Neubauer, R. Georgii, and P. Böni, Science **323**, 915 (2009).
[2] X. Yu, Y. Onose, N. Kanazawa, J. Park, J. Han, Y. Matsui, N. Nagaosa, and Y. Tokura, Nature **465**, 901 (2010).
[3] W. Münzer, A. Neubauer, T. Adams, S. Mühlbauer, C. Franz, F. Jonietz, R. Georgii, P. Böni, B. Pedersen, M. Schmidt, *et al.*, Phys. Rev. B **81**, 041203 (2010).
[4] S. Woo, K. Litzius, B. Krger, M.-Y. Im, L. Caretta, K. Richter, M. Mann, A. Krone, R. M. Reeve, M. Weigand, P. Agrawal, I. Lemesh, M.-A. Mawass, P. Fischer, M. Klui, and G. S. D. Beach, Nature Materials **15**, 501 (2016).
[5] S. Gao, H. D. Rosales, F. A. Gómez Albarracín, V. Tsurkan, G. Kaur, T. Fennell, P. Steffens, M. Boehm, P. Čermák, A. Schneidewind, *et al.*, Nature **586**, 37 (2020).
[6] N. Nagaosa and Y. Tokura, Nature Nanotechnology **8**, 899 (2013).
[7] A. Fert, V. Cros, and J. Sampaio, Nature Nanotechnology **8**, 152 (2013).
[8] D. Pinna, F. Abreu Araujo, J.-V. Kim, V. Cros, D. Querlioz, P. Bessiere, J. Droulez, and J. Grollier, Phys. Rev. Applied **9**, 064018 (2018).
[9] J. Zázvorka, F. Jakobs, D. Heinze, N. Keil, S. Kromin, S. Jaiswal, K. Litzius, G. Jakob, P. Virnau, D. Pinna, K. Everschor-Sitte, L. Rózsa, A. Donges, U. Nowak, and M. Kläui, Nature Nanotechnology **14**, 658 (2019).
[10] N. Mohanta, E. Dagotto, and S. Okamoto, Phys. Rev. B **100**, 064429 (2019).
[11] D. S. Kathyat, A. Mukherjee, and S. Kumar, Phys. Rev. B **103**, 035111 (2021).
[12] J. H. Han, J. Zang, Z. Yang, J.-H. Park, and N. Nagaosa, Phys. Rev. B **82**, 094429 (2010).
[13] A. O. Leonov and M. Mostovoy, Nature Communications **6**, 8275 (2015).
[14] A. Bogdanov and U. Rößler, Phys. Rev. Lett. **87**, 037203 (2001).
[15] B. Binz, A. Vishwanath, and V. Aji, Phys. Rev. Lett. **96**, 207202 (2006).
[16] U. K. Roessler, A. Bogdanov, and C. Pfleiderer, Nature **442**, 797 (2006).
[17] H. D. Rosales, D. C. Cabra, and P. Pujol, Phys. Rev. B

92, 214439 (2015).
[18] X. Zhang, Y. Zhou, and M. Ezawa, Scientific reports **6**, 24795 (2016).
[19] B. Göbel, A. Mook, J. Henk, and I. Mertig, Phys. Rev. B **96**, 060406 (2017).
[20] S. A. Osorio, M. B. Sturla, H. D. Rosales, and D. C. Cabra, Phys. Rev. B **100**, 220404(R) (2019).
[21] M. E. Villalba, F. A. Gómez Albarracín, H. D. Rosales, and D. C. Cabra, Phys. Rev. B **100**, 245106 (2019).
[22] Y. Nishikawa, K. Hukushima, and W. Krauth, Phys. Rev. B **99**, 064435 (2019).
[23] P. Huang, T. Schönenberger, M. Cantoni, L. Heinen, A. Magrez, A. Rosch, F. Carbone, and H. M. Rønnow, Nature Nanotechnology **15**, 761 (2020).
[24] J. Zázvorka, F. Dittrich, Y. Ge, N. Kerber, K. Raab, T. Winkler, K. Litzius, M. Veis, P. Virnau, and M. Kläui, Advanced Functional Materials **30**, 2004037 (2020).
[25] N. Mohanta, A. D. Christianson, S. Okamoto, and E. Dagotto, Communications Physics **3**, 1 (2020).
[26] P. Baláž, M. Paściak, and J. Hlinka, Phys. Rev. B **103**, 174411 (2021).
[27] M. Ezawa, Phys. Rev. B **83**, 100408 (2011).
[28] J. Knolle and R. Moessner, Annual Review of Condensed Matter Physics **10**, 451 (2019).
[29] L. Messio, C. Lhuillier, and G. Misguich, Phys. Rev. B **87**, 125127 (2013).
[30] Y.-C. He, D. N. Sheng, and Y. Chen, Phys. Rev. Lett. **112**, 137202 (2014).
[31] K. Essafi, O. Benton, and L. D. Jaubert, Nature Communications **7**, 1 (2016).
[32] D. A. Huse and A. D. Rutenberg, Phys. Rev. B **45**, 7536 (1992).
[33] K. Essafi, O. Benton, and L. D. C. Jaubert, Phys. Rev. B **96**, 205126 (2017).
[34] A. O. Leonov, C. Pappas, and I. I. Smalyukh, Phys. Rev. B **104**, 064432 (2021).
[35] J. T. Chalker, P. C. W. Holdsworth, and E. F. Shender, Phys. Rev. Lett. **68**, 855 (1992).
[36] S. Guitteny, J. Robert, P. Bonville, J. Ollivier, C. Decorse, P. Steffens, M. Boehm, H. Mutka, I. Mirebeau, and S. Petit, Phys. Rev. Lett. **111**, 087201 (2013).
[37] S. Zhang, H. J. Changlani, K. W. Plumb, O. Tchernyshyov, and R. Moessner, Phys. Rev. Lett. **122**, 167203 (2019).
[38] J. Robert, B. Canals, V. Simonet, and R. Ballou, Phys. Rev. Lett. **101**, 117207 (2008).
[39] J. G. Rau and M. J. P. Gingras, Nature Communications **7**, 12234 (2016).
[40] M. Udagawa, L. D. C. Jaubert, C. Castelnovo, and R. Moessner, Phys. Rev. B **94**, 104416 (2016).
[41] H. Yan, R. Pohle, N. Shannon, *et al.*, Phys. Rev. B **98**, 140402 (2018).
[42] C. Balz, B. Lake, J. Reuther, H. Luetkens, R. Schnemann, T. Herrmannsdrfer, Y. Singh, A. T. M. Nazmul Islam, E. M. Wheeler, J. A. Rodriguez-Rivera, T. Guidi, G. G. Simeoni, C. Baines, and H. Ryll, Nature Physics **12**, 942 (2016).
[43] R. Pohle, H. Yan, and N. Shannon, Phys. Rev. B **104**, 024426 (2021).
[44] T. Mizoguchi, L. D. Jaubert, R. Moessner, and M. Udagawa, Phys. Rev. B **98**, 144446 (2018).
[45] S. Zhang, J. Zhang, Y. Wen, E. M. Chudnovsky, and X. Zhang, Applied Physics Letters **113**, 192403 (2018).
[46] A. Derras-Chouk and E. M. Chudnovsky, Journal of Physics: Condensed Matter **33**, 195802 (2021).
[47] D. Chakrabartty, S. Jamaluddin, S. K. Manna, and A. K. Nayak, "Uncovering the skyrmion bubble magnetic states in centrosymmetric kagome magnet Mn4Ga2Sn," (2021), arXiv:2112.11259.
[48] J. L. Jacobsen, Journal of Physics A: Mathematical and Theoretical **40**, 14667 (2007).
[49] "Note that we have extended Jacobsen's definition of hamiltonian chains to include single vertices, i.e. skyrmions.".
[50] P. J. Flory, *Principles of Polymer Chemistry* (Cornell Univ. Press, 1971).
[51] K. Dill, Protein Science **8**, 1166 (1999).
[52] A. A. Abate, C. M. Piqueras, and D. A. Vega, Macromolecules **54**, 1639 (2021).
[53] H. J. Changlani, D. Kochkov, K. Kumar, B. K. Clark, and E. Fradkin, Phys. Rev. Lett. **120**, 117202 (2018).
[54] K. Lee, R. Melendrez, A. Pal, and H. J. Changlani, Phys. Rev. B **101**, 241111 (2020).